Molecular Cell, Volume *72*

Supplemental Information

Critical Role of the UBL Domain in Stimulating the E3 Ubiquitin Ligase Activity of UHRF1 toward Chromatin

Benjamin M. Foster, Paul Stolz, Christopher B. Mulholland, Alex Montoya, Holger Kramer, Sebastian Bultmann, and Till Bartke

SUPPLEMENTAL FIGURE LEGENDS

Figure S1, related to Figure 1. UHRF1 forms a monomer in solution. (A) XL-MS diagram of UHRF1$^{\Delta MW}$ visualised using xVis. Domains are annotated and colour-coded are as in Figure 1A. (B) Size-exclusion chromatograms of UHRF1 (wildtype, ΔMW and ΔUBL) using a Superdex 200 16/60 column. The column was calibrated with markers of known size (GE Healthcare). (C) Recombinant UHRF1 (wildtype and ΔMW) was treated with increasing amounts of glutaraldehyde to test if distinct multimeric forms could be distinguished. HP1α and chicken albumin were used as positive and negative controls, respectively. The reactions were quenched with SDS-loading buffer and analysed by 10% SDS-PAGE stained with Coomassie Brilliant Blue.

Figure S2, related to Figure 2. The UBL-domain does not directly affect the nucleosome-binding characteristics of UHRF1. (A) Schematic annotation of the domain architecture of the full-length UHRF1 protein and the truncated versions that were tested in nucleosome EMSAs. The white box at the very N-terminus of the ΔMW mutant indicates four amino acids (RPDP) that replace the N-terminal two amino acids Met-Trp. (B) Representative nucleosome electrophoretic mobility shift assays (EMSAs) for UHRF1^{WT}, UHRF1$^{\Delta MW}$, ΔUBL, a short fragment (118-621) and the His$_6$-UBL with H3K9me3-modified mono-nucleosomes. Binding was analysed by 5% native PAGE in 0.2x TBE and staining with ethidium bromide or SYBR safe. (C) EMSA band shift experiments were conducted as in (B) using nucleosomes assembled from unmodified or H3K9me3-modifed octamers and/or CpG hemi-methylated 601-DNA (3x hemi-meth CpGs in the 3' linker) and the relative amount of unbound mono-nucleosome was quantified by ImageJ in >3 independent experiments. The mean was plotted with error bars representing the standard error of the mean (SEM) and a non-linear regression curve used to fit the data points. From this fit, the amount of UHRF1 to bind half of the mono-nucleosomes (Apparent K_d) was calculated (see Table S2).

Figure S3, related to Figure 2. UHRF1 E3-ubiquitin ligase activity controls. (A) Identification of a suitable E2-partner for UHRF1 E3-ubiquitin ligase activity. E3 auto-ubiquitylation assay with UHRF1$^{\Delta MW}$ and a selection of E2-conjugating enzymes (1 – UBE2L3; 2 – UBE2N/UBE2V1; 3 – UBE2C; 4 – UBE2E3; 5 – UBE2H; 6 – UBE2E1; 7

– UBE2R1; 8 – UBE2D1; 9 – UBE2D2; 10 – UBE2D3, Boston Biochem). UHRF1 auto-ubiquitylation was detected by anti-ubiquitin Western blot with high molecular weight species indicating UHRF1 E3 activity. A Coomassie Brilliant Blue-stained gel was used as a loading control for His_6-UBE1 and to visualise the disappearance of unmodified UHRF1 upon poly-auto-ubiquitylation. The $UHRF1^{\Delta MW}$ mutant lacking the first two amino acids was used in these assays. (B) UHRF1 E3 activity is dependent on the presence of the E1 and E2 enzymes, ubiquitin and ATP. UHRF1 auto-ubiquitylation (smear at high molecular weights when probed against ubiquitin) and H3-ubiquitylation only occurs when all the necessary components are present for UHRF1 E3 activity. (C) UHRF1 concentration-dependent conversion of histone H3 to H3-Ub by the UHRF1 E3 activity. The titration was as follows: 0 μM, 0.05 μM, 0.1 μM, 0.2 μM and 0.4 μM. (D) Schematic representation of the ubiquitylated lysine residues identified on histone H3. H3 Lys-18 and Lys-23 were the most relatively abundant peptides on histone H3 with $UHRF1^{WT}$ (Lys-14 and Lys-27 ubiquitylation was also identified). Additional H3-ubiquitylation was identified at Lys-9, Lys-56 and Lys-79 in similar assays using $UHRF1^{\Delta MW}$ (see Figure S5C). Analysis was performed by mass spectrometry. Spectra for the modified peptides are provided in Data S1. (E) An E3 assay ($UHRF1^{WT}$, +/- ATP) was analysed by Western blot with antibodies against UHRF1 to verify that the high molecular weight smear in the HA-blots is auto-ubiquitylated UHRF1 and not long poly-ubiquitin chains. (F) Quantification of the E3 assays shown in Figure 2A. Assays were carried out in triplicate and the levels of H3 species (as observed by Western blot) were quantified using ImageJ. The mean relative levels of H3 and ubiquitylated H3 species are indicated for mono-, di- and tetra-nucleosomes and 12x187bp chromatin arrays. Error bars indicate the standard error of the mean (SEM).

Figure S4, related to Figure 2. UHRF1 E3-ubiquitin ligase time courses on modified chromatin substrates. (A) E3 time course assays were carried out to directly compare UHRF1 ubiquitin ligase activity in the presence of 12x187bp chromatin arrays or mono-nucleosomes containing un- or fully CpG methylated DNA and either unmodified or H3K9me3 octamers as indicated. E3 assays with unmodified arrays or nucleosomes from Figure 2A are shown for comparison. Filled circles represent symmetrically methylated CpG DNA and a blue block tri-methylated Lys-9 on histone H3. There is some increase in E3 activity in the presence of H3K9me3-

containing mono-nucleosomes and 12x187bp arrays, whilst increased UHRF1 auto-ubiquitylation but decreased H3 ubiquitylation was detected with fully CpG-methylated DNA within both mono-nucleosomes and 12x187bp arrays. (B) E3 assays were carried out on mono-nucleosomes containing hemi-methylated CpGs within the linker/overhang flanking the nucleosome positioning sequence in the context of unmodified and H3K9me3-containing octamers. Hemi-methylated CpGs are represented by empty circles. E3 assays on nucleosomes containing three hemi-methylated CpGs in the 3'-linker exhibited no detectable H3-ubiquitylation whilst a single hemi-methylated CpG in the 5'-linker enabled H3-ubiquitylation similar to mono-nucleosomes containing CpG-methylated DNA. In both cases, UHRF1 auto-ubiquitylation was increased when compared to other chromatin or nucleosome substrates.

Figure S5, related to Figure 3. UHRF1$^{\Delta MW}$ exhibits greater auto-ubiquitylation than UHRF1^{WT} and is non-responsive to relevant pre-existing chromatin marks. (A) E3 time course assays were carried out to directly compare UHRF1$^{\Delta MW}$ ubiquitin ligase activity in the presence of 12x187bp chromatin arrays containing un- or fully CpG methylated array DNA and either unmodified or H3K9me3 octamers as indicated (schematic modifications are represented as in Figure S4). There was no substantial increase in rate or amount of activity detectable by western blot when comparing unmodified against H3K9me3 octamers or with methylated chromatin array DNA in the context of UHRF1$^{\Delta MW}$. (B) Western blot analysis of E3 assays carried out with wild type or NoK (all lysine residues mutated to arginine) ubiquitin to investigate whether activity is stimulated by the formation of poly-ubiquitin chains on UHRF1. H3-ubiquitylation is relatively unaffected in UHRF1^{WT} assays (1 hour at 25°C) although there are likely poly-ubiquitin species starting to form when analysing the α-ubiquitin blot. Multi-mono-ubiquitylation but not poly-auto-ubiquitylation on UHRF1$^{\Delta MW}$ (90 min at 25°C) in the NoK mutant can be detected by the reduced smear when probed with antibodies to ubiquitin. Ubiquitylation on histone H3 was unaffected indicating that H3 is decorated by two mono-ubiquitins and that poly-ubiquitylation of UHRF1 is not required to stimulate activity. (C) Schematic representation of the residues and regions of UHRF1$^{\Delta MW}$ and of histone H3 that are ubiquitylated in UHRF1$^{\Delta MW}$ E3 assays. The UHRF1$^{\Delta MW}$ mutant ubiquitylates a broader spectrum of lysines on histone H3 than

UHRF1^{WT} (see Figure S3D) indicating a potential loss of specificity or fidelity of targeting ubiquitin to the correct lysines. Analysis was performed by mass spectrometry. Spectra for the modified peptides are provided in Data S1.

Figure S6, related to Figure 6. The Phe-46 to Ala mutation in the UBL domain reduces E3 ubiquitylation activity but does not affect chromatin-binding by UHRF1. (A) E3 time-course assays were carried out with the indicated UBL or RING-domain mutants and followed over 30 min (for comparison, WT and H730A are from Figure 2A and 2B, respectively). Samples were analysed by Western blot and probed with an antibody to histone H3 and the HA-tagged ubiquitin. Unmodified 12x187bp chromatin arrays were used as substrate. (B) Chromatin EMSA using the unmodified 12x187bp array as a substrate. Increasing amounts of UHRF1 as labelled were titrated into the reaction and the shift in migration of the array was analysed by 0.7% agarose gel electrophoresis in 0.2x TB. Gels were stained with ethidium bromide or SYBR safe. (C) Quantification of the experiments shown in (B). Shown are the mean values of three independent experiments. The mean was plotted with error bars representing the standard error of the mean (SEM). From this fit, the amount of UHRF1 to bind half of the 12x187bp chromatin arrays (Apparent K_d) was calculated (see Table S2).

Figure S7, related to Figure 7. Characterisation of *Uhrf1* CRISPR/Cas9 knock-in mutants. (A) Generation of *Uhrf1*^{F46A} and *Uhrf1*^{H730A} mutant mouse ES cells. The upper panel is a schematic representation of the CRISPR/Cas9 gene editing strategy applied to mutate the UBL and RING-domain of *Uhrf1*. Respective gRNA targeting and restriction enzyme recognition sites for restriction fragment length polymorphism (RFLP) are depicted. The lower panel shows the genotyping of *Uhrf1*^{F46A} and *Uhrf1*^{H730A} mutants as performed via RFLP screen and confirmation of the correct insertion of point mutations by Sanger Sequencing. (B) A second set of clones tested for DNMT1 localization during DNA replication assessed by immunofluorescence in *Uhrf1*^{WT}, *Uhrf1*$^{-/-}$ and *Uhrf1* mutant (*Uhrf1*^{H730A} clone 3B4 and *Uhrf1*^{F46A} clone 2E4) mESCs. Fluorescently labelled EdU was used to visualize newly synthesized DNA and to monitor cells in S phase. Scale bar for individual nuclei and pool of cells is 5 μm and 10 μm, respectively.

Foster et al. Figure S1

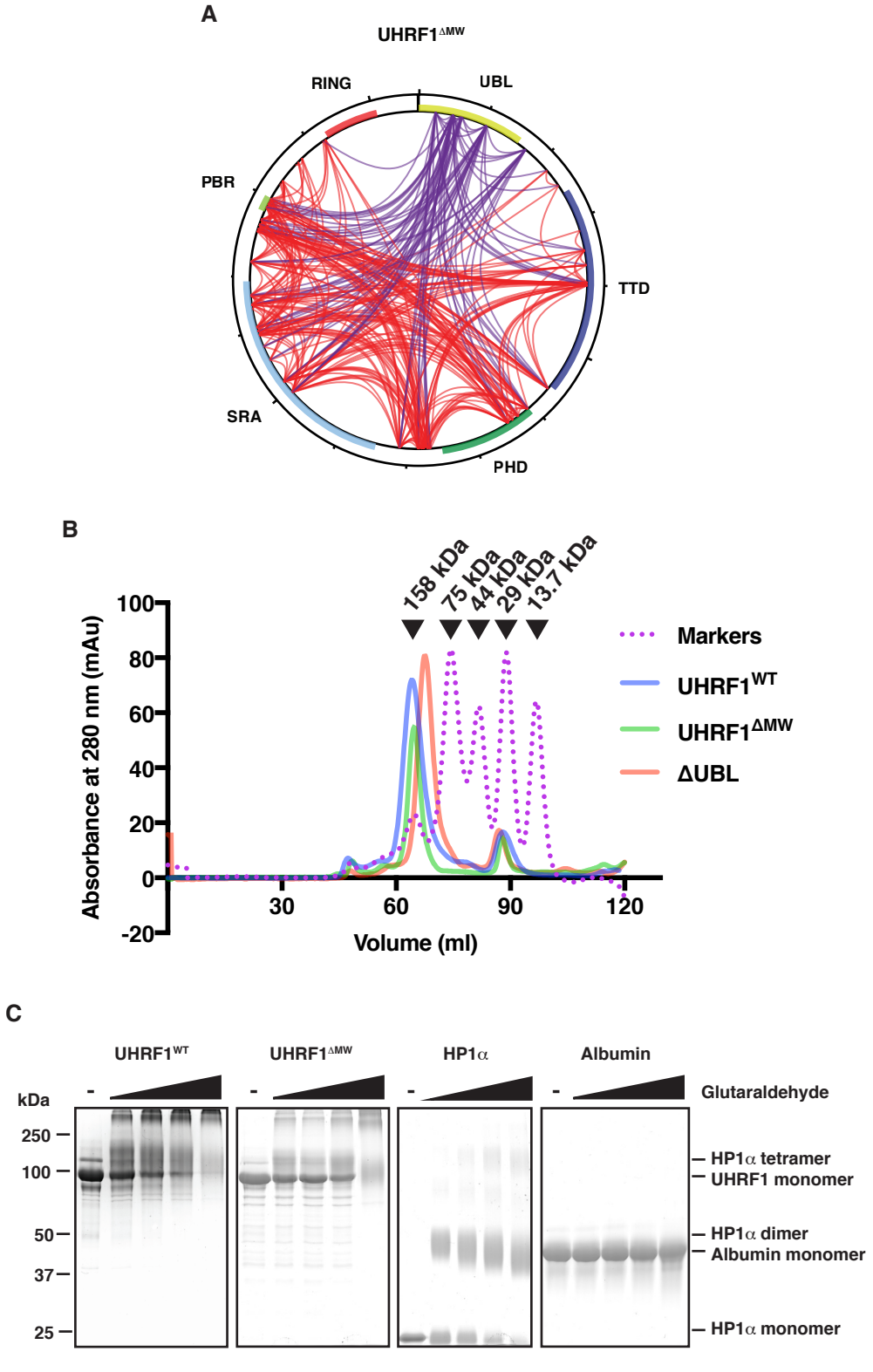

Foster et al. Figure S2

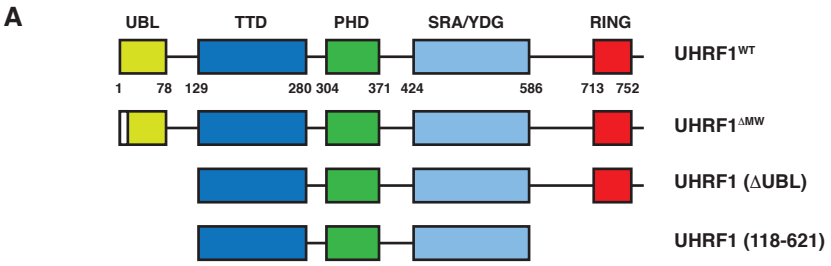

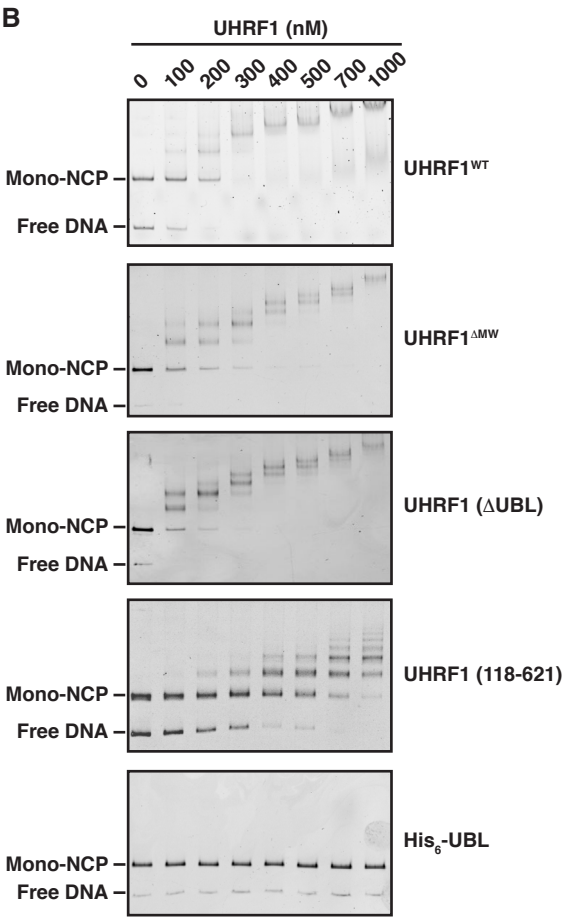

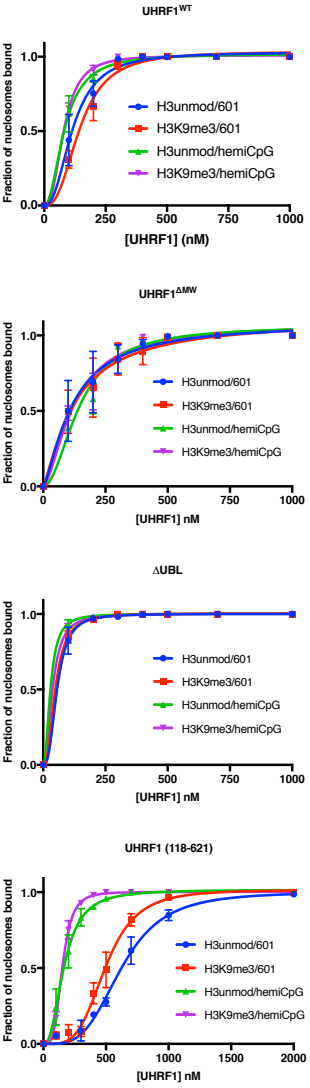

Foster et al. Figure S3

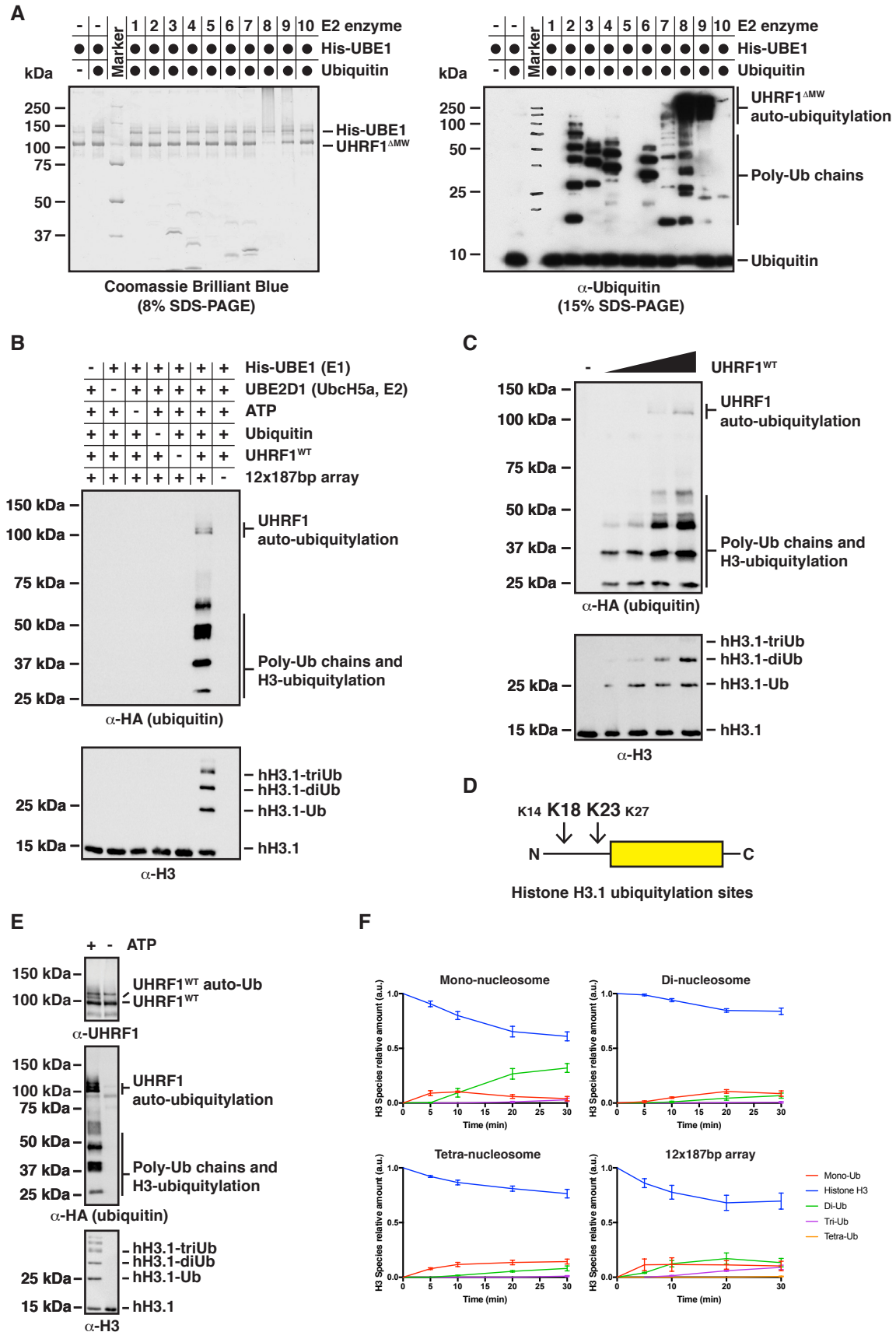

Foster et al. Figure S4

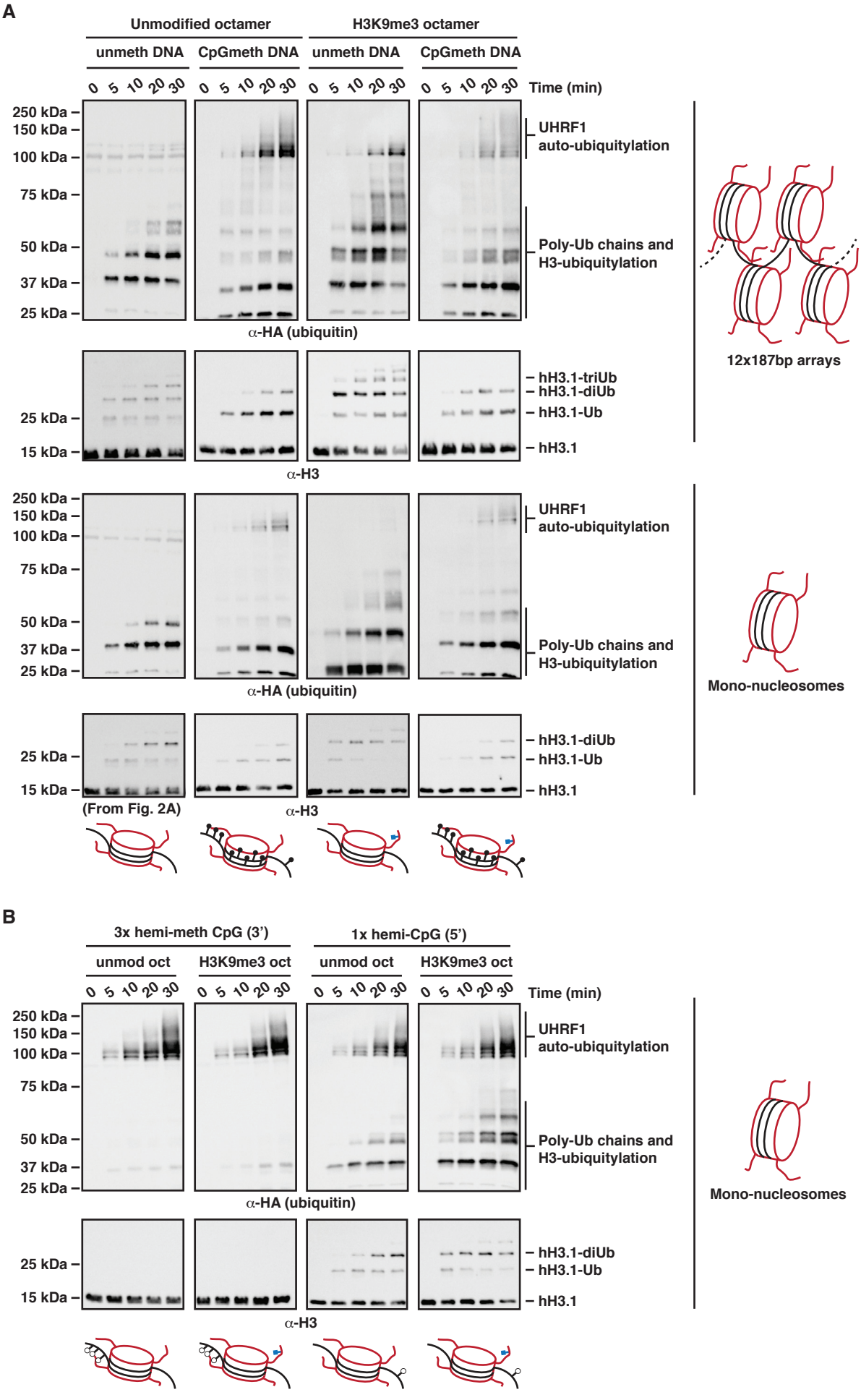

Foster et al. Figure S5

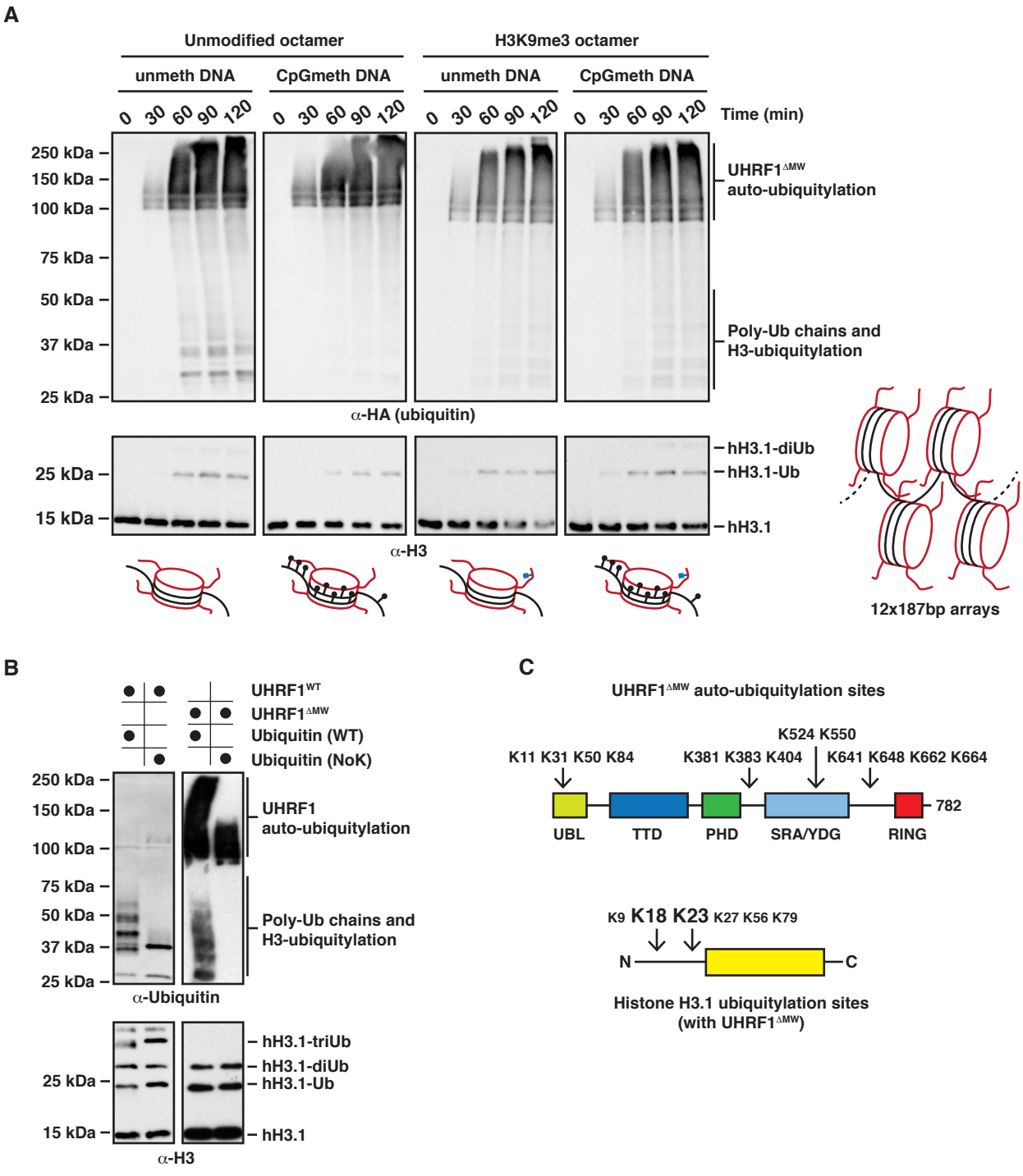

Foster et al. Figure S6

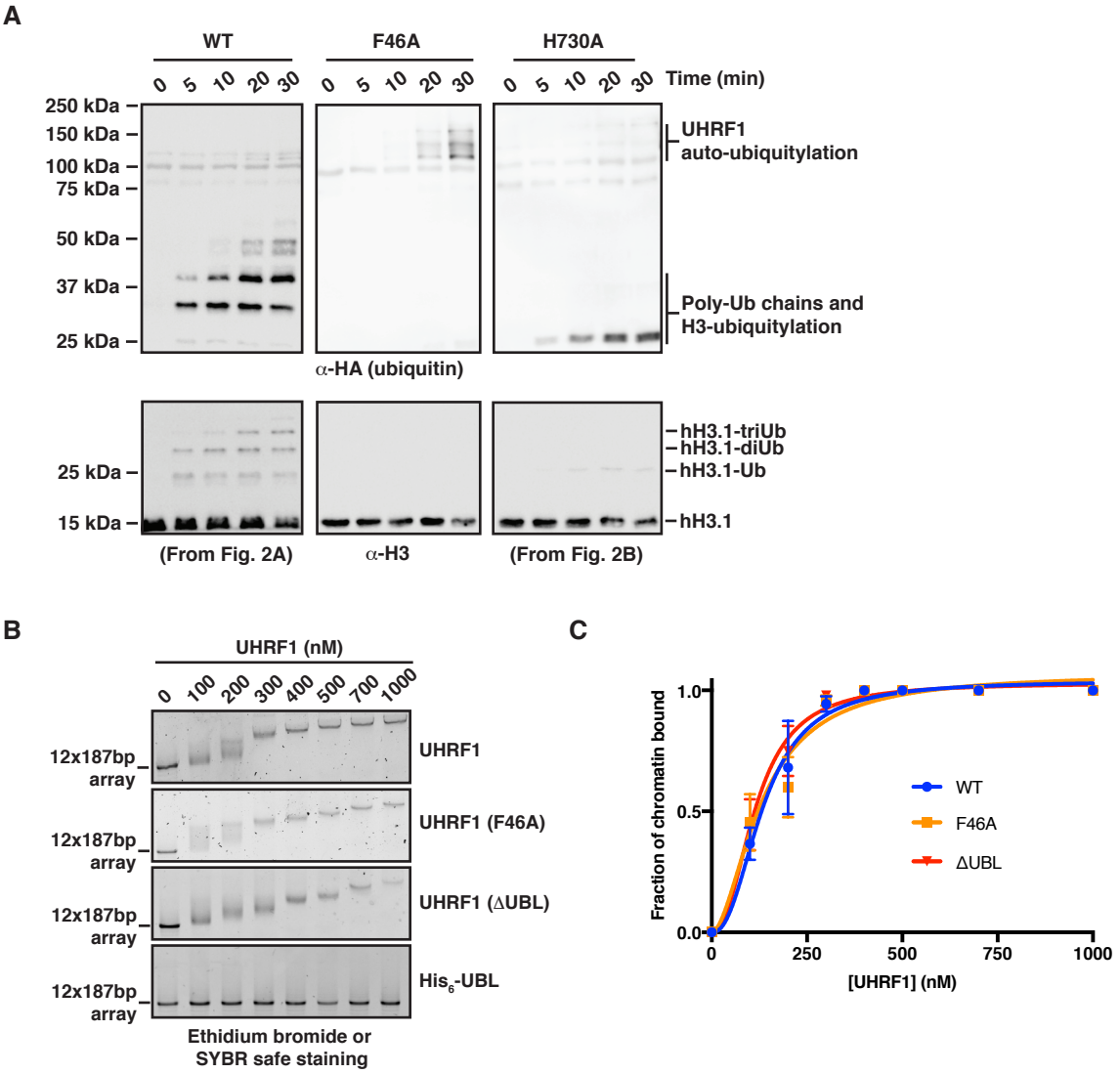

Foster et al. Figure S7